# Chapter 4

# Novel Real-Valued Improved Coral-Reef Optimization Algorithm for Optimal Integration of Classified Distributed Generators

## 4.1 Introduction

The previous chapter dealt with the optimal integration of various combination cases of the Type-1, Type-2, and Type-3 DGs using the PSO-GSA algorithm. This chapter, with the objective of power loss minimization, proposes a novel hybrid meta-heuristics approach: Particle Swarm Optimization-Coral Reef Optimization (PSO-CRO) for identifying an optimum positioning and rating of Type-1, Type-2 & Type-3 DGs (at 0.82 optimal power factor) in IEEE 33-bus, 69-bus & 118-bus Radial Distributed Systems (RDS). Furthermore, the results from the proposed hypothesis are compared with some of the prevalent peers, namely, PSO, CRO, Gravitational Search Algorithm (GSA), PSO-GSA, and PSO-Grey Wolf Optimization (PSO-GWO), etc. The results of the proposed algorithm are also compared with the results of the GAMS/CONOPT commercial solver.

## 4.2 Problem Formulation

It is imperative to provide a suitable allocation of DG with appropriate size as the improper siting and sizing of DGs in the distribution network causes increased power loss, and operating cost, reduces energy transmission capability, and leads to under utilization of resources. The objective of the proposed approach of DG placement is to minimize total active power loss subject to various constraints like load flow equations, voltage constraints, current constraints, and DG size constraints. Power loss represented in Chapter 2 by (2.1) has been considered as the objective function that has been minimized using the PSO-CRO algorithm under the constraints given in Section 2.2.5 (Chapter-2) and Section 3.2 (Chapter-3).

## 4.3 Optimal Placement of DGs

A novel hybrid metaheuristic optimization technique PSO-CRO is proposed for optimal integration of classified DGs. The proposed approach exhibits improved performance, flexibility in decision-making, intelligence, and high scalable property over conventional optimization approaches. PSO-CRO is flexible in decision making and it determines the alternate optimal solutions for a problem. On the contrary, a conventional algorithm's flexibility in decision-making depends on the user's understanding of the problem. Intelligence in the proposed approach involves a bottom-up approach, which generates simple basic rules, whereas in conventional algorithm rules generation is problem dependent. the improved CRO approach is highly scalable but conventional algorithms are scalable up to a certain extent. Less computational time, cost-effectiveness, ease of programming, and lesser mathematical complexity are the advantages of the improved CRO approach over conventional optimization methods.

This chapter presents the application of the proposed PSO-CRO approach for finding the optimal location and size of DG for minimum system active power loss. It is apparent from (2.1) (in Chapter-2) that real power loss ($P_{Loss}$) is a function of power injected by DG placed at a bus. Thus, injected power as well as the location of DG can be varied by the

proposed approach to get minimum real power loss in the network. The proposed approach provides information in the form of the optimal size and location of DG. In this work Type-1, Type-2, and Type-3 DGs are optimally integrated in 33-bus, 69-bus, and 118-bus IEEE networks to minimize the objective function, using the PSO-CRO approach. To minimize the objective function, variables in the decision vector considered in the system are given below:

$$D_{var} = [DG_{loc} \qquad DG_{size}] \tag{4.1}$$

where, decision variables $DG_{loc}$ and $DG_{size}$ are the DG location and DG size.

### 4.3.1 Proposed Novel Approach of DG Placement through Particle Swarm Optimization-Coral Reef Optimization (PSO-CRO) Algorithm

The proposed algorithm provides a co-evolutionary hybridization of Particle Swarm Optimization (PSO) and Coral Reef Optimization (CRO) techniques [105] for determining the optimal location and size of Type-1, Type-2, and Type-3 DGs to be placed in the system. The methodology blended the high exploration capability of PSO with the excellent exploitation proficiency of Coral Reef Optimization (CRO). It is termed as co-evolutionary as both the algorithms run in tandem to achieve the solution for a given optimization problem.

#### Corals and Reef Formation

The corals belong to the Cnidaria phylum. Hundreds of such corals form a reef. Thus, let $\wedge$ represent an N × M reef grid. It is assumed that each block (n, m) of the grid is able to house a coral $E_{i,j}$, representing the different feasible solutions of a given problem.

#### Problem Initialization

Initially, some squares of $\wedge$ are set to be occupied by corals, and some are left empty. This initial ratio $\rho_0$ of the free square to occupied squares is in the range $0 < \rho_0 < 1$. Consider

Fig. 4.1, for a grid of 5×5 size, the shaded squares indicate the existence of a coral and the hole represents the absence of them. The occupied places are 14 and the non-occupied are 11. Thus, $\rho_0 = 11/14$, which is approximately equal to 0.785. Each feasible solution is

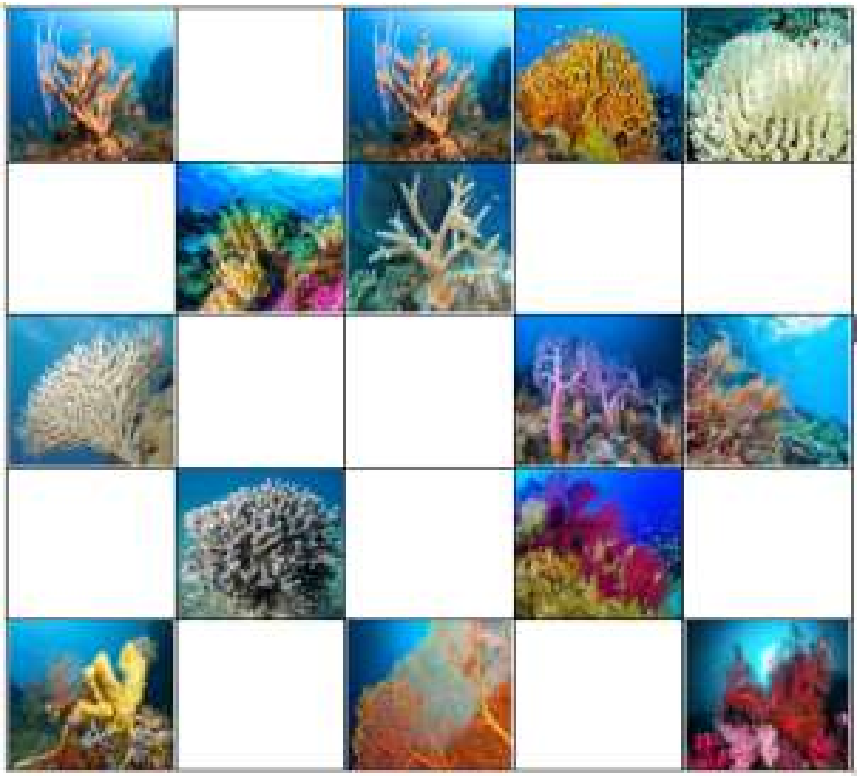

Fig. 4.1 Coral and empty spaces in a reef

accompanied by its health, which is the value of the objective function when the solution is substituted into the given function. It is imperative that for a maximization problem, solutions that have better health survive, whereas, weaker solutions perish gradually.

Subsequently, the second phase of reef formation through reproduction is carried out which includes modeling of sexual reproduction (broadcast spawning and brooding) and asexual reproduction (budding). Lastly, the new corals fight for their place in the reef modeled by the depredation process.

The pseudo-code for the proposed approach is shown in Fig. 4.2. In Fig. 4.2 n is the total number of buses in the system, ESlarvae represents the coral larvae production after External Sexual Reproduction (i.e. Broadcast Spawning and Brooding). ISlarvae

represents the coral larvae production after Asexual Reproduction. $p_{best}$, and $g_{best}$ are the local best and global best positions of the produced larvae in unit time. $c_1$, $c_2$, and $c$ are the cognitive (individual), social (group) and overall learning rates, respectively.

**Start PSO-CRO**
1: Initialize particle swarm and coral reef
2: Calculate fitness
3: Initialize *gbest*
4: **While** (stopping criterion is not met)
5: **For** *bus= 1 to n*
6: Perform **Broadcast Spawning** to obtain *ESlarvae*
7: Perform **Reef Brooding** to obtain *ISlarvae*
8: $v = c \times \left( \left( w \times v \right) + c_1 \times rand \times \left( p_{best} - ESlarve \right) + c_2 \times rand \times \left( g_{best} - ESlarve \right) \right)$
Update *ESlarvae:*
*ESlarve=ESlarvae+v*
9: Update *ISlarvae:*
$v = c \times \left( \left( w \times v \right) + c_1 \times rand \times \left( p_{best} - ISlarve \right) + c_2 \times rand \times \left( g_{best} - ISlarve \right) \right)$
*ISlarve=ISlarvae+v*
10: Apply the range constriction on the *ESlarvae & ISlarvae*
11: Calculate fitness for *ESlarvae & ISlarvae*
12: Perform **Larvae Setting**
13: Perform **Reef Budding**
14: Perform **Larvae Setting**
15: Perform **Extreme Depredation**
16: Update reef fitness
17: Update $g_{best}$
18: **End For**
19: **End While**
**Stop PSO-CRO**

Fig. 4.2 Pseudo-code for the proposed PSO-CRO Method

**Global Best Solution**

The exploration feature of the PSO has been incorporated to improve the efficiency of the CRO. Once the fitness is determined, the global best variable is used to retain the value of the solution that generates the best fitness value. Later this value is used to improve the quality of the solutions generated through sexual reproduction.

### Sexual Reproduction

(a) External Sexual Reproduction (Broadcast Spawning): This phenomenon involves a two-step approach explained as follows:

(1) In any given iteration $i$, a fraction of the corals is selected as the broadcast spawners. This fraction is denoted by, $F_b$, and the remaining $(1 - F_b)$ reproduce through brooding.

(2) The spawners are selected using the fitness proportionate approach to form couples, which then form a larva through the crossover.

(b) Internal Sexual Reproduction (Brooding): The $(1 - F_b)$ brooders form larvae by a random mutation process.

### Larvae Setting

The larvae generated through any of the above-mentioned processes now try to settle in the reef. The setting process of larvae depends on their fitness value. If the reef space is empty, the larvae simply occupy it, but if another coral preoccupies the square then the one with a better fitness value gets the space. A larva is given k attempts to search and settle in a square in the grid. The larvae perish if it fails in k attempts.

### Asexual Reproduction

In Budding, firstly, all the corals are sorted based on their fitness values out of which a fraction $F_a$ imitates itself to form new larvae that again try to settle in the grid.

### Depredation

The depredation process involves the elimination of weaker solutions in the group. After the reproduction process is completed, a fraction $F_d$ of the corals in the reef are depredated and fresh empty spaces are formed.

The above-mentioned process is repeated until the stopping criteria is satisfied. The algorithm for the hybrid PSO-CRO approach is given below.

**Algorithm**

Step 1. Initialization

Initially, the parameters of both CRO and PSO are initialized. The size of the reef is selected as per the problem's requirement and the corals (feasible solutions) are randomly initialized and settled into the reef.

Step 2. Fitness evaluation

Fitness for each coral in the reef is evaluated by substituting the value of each individual set of solutions in the objective function.

Step 3. $g_{best}$ Updation

The solution that has best fitness value is stored in the $g_{best}$ variable.

Step 4. Broadcast Spawning

Randomly selected corals depending on the value of $F_b$ are selected as the spawners. Amongst these spawners, pairing is done for the crossover process, and a spawner is allowed to parent a larva only once in an iteration. The couple selection is done using the roulette-wheel selection approach.

The pseudocode code for broadcast spawning is given in Fig. 4.3 below. In Fig. 4.3, spawners are selected to reproduce a larva through the crossover. Two spawner groups (i.e. spawner1 and spawner2) are selected for crossover purposes. In the real-valued mutation equation, B and mask are mutation variables that range between zero and one.

**Start Broadcast Spawning**

1: Divide Spawners into two groups

2: Generate *ESlarvae*

$$ESlarvae1 = spawners1 * (1 - mask) * \frac{(1-B)}{2} + spawners2 * mask * \frac{(1+B)}{2}$$

$$ESlarvae2 = spawners1 * (1 - mask) * \frac{(1+B)}{2} + spawners2 * mask * \frac{(1-B)}{2}$$

$$ESlarvae = [ESlarvae1; ESlarvae2]$$

**Stop Broadcast Spawning**

Fig. 4.3 Pseudocode for Broadcast Spawning

Step 5. Reef Brooding

The $(1-F_b)$ corals reproduce asexually by means of a random mutation process. These larvae are then fit for settlement in the reef.

The pseudo-code code for Reef Brooding is given in Fig. 4.4. In Fig. 4.4 M and m are the maximum and minimum values of the larvae that participated in brooding, S is the intermediate variable for saving the results of the comparison, r is the random number generated between zero and one and D is the scaling factor. Brooders are the spawners participating in Internal Sexual Reproduction (Brooding). The larvae are then updated

**Start reef brooding**
1: Select (1-$F_b$) brooders randomly
2: Set eta=0.2
3: M=max(brooders)
4: m=min(brooders)
5: **for** all brooders
6: **if** M=m
7: **then** S=M
8: **else** S=abs(M-m)
9: **End if**
10: Generate random no. r
11: **if** r≥0.5
12: **then** $D=(1-2*r)^{1/(eta+1)}$
13: **else** $D=(1-2*r)^{1/(eta+1)}-1$
14: **End if**
15: larvae=brooders+S*D
16: **End for loop**
**Stop reef brooding**

Fig. 4.4 Pseudo-code for the proposed Reef Brooding

with the $g_{best}$ information as well to enhance their quality.

Step 6. Fitness evaluation

The fitness of each larva formed either by broadcasting or by brooding is evaluated.

Step 7. Larvae setting

Randomly selecting a position in the reef, the larvae try to settle in the reef. If the (n, m) square is empty the larva will settle irrespective of its fitness value. If the (n, m) is already

occupied, the larva can only settle, if it has a better fitness value than the coral residing there. A maximum of k attempts is given to a larva to try to occupy a space in the reef, in case of failure the larva perishes.

The pseudo-code for the larvae setting is shown in Fig. 4.5.

**Start Larvae Setting**
1: Arrange all larvae randomly
2: Each larva is assigned a place in the reef to settle
3: **for** each larva
4: **if** the reef is empty
5: **then** larva occupies
6: **End if**
7: **if** the place is occupied
8: **then if** the larva is better than the coral it occupies the space
9: **End if**
10: Otherwise, a larva is discarded after 3 unsuccessful attempts
11: **End for**
**Stop Larvae Setting**

Fig. 4.5 Pseudo-code for larvae setting

Step 8. Reef Budding

In budding, all the corals in the reef are sorted as a function of their fitness value, and a fraction $F_a$ duplicates itself and tries to settle in a different position in the reef by following the larvae setting process.

The pseudo-code for reef budding is shown in Fig. 4.6.

**Start Reef Budding**
1: Select those reefs which have occupied space & their fitness
2: Sort them in descending order of fitness
3: Select $F_a$ reef as larvae
**Stop Reef Budding**

Fig. 4.6 Pseudo-code for Reef Budding

Step 9. Depredation

At the end of each reproduction stage, $F_d$ fraction of corals get eliminated, generally that have the worst health in the reef.

The pseudo-code for depredation is shown in Fig. 4.7. In Fig. 4.7, $P_i$ is the random probability of depredation for each coral and $P_d$ is the threshold value of the probability of depredation.

```
Start depredation
1: Sort the corals in ascending order based on their fitness
2: Generate random number Pi for each coral
3:          for all corals
4:                  if Pi>Pd
5:                  then eliminate the coral
6:                  End if
7:          End for
Stop depredation
```

Fig. 4.7 Pseudo-code for Depredation

If the stopping criteria is met the process may be terminated else, it is repeated from step 3. The flowchart for optimal siting and sizing of DG using the PSO-CRO algorithm is shown in Fig.4.8. In this flowchart $DG_{loc}$ represents DG location and $DG_{size}$ represents DG size. Power loss ($P_{Loss}$) defined by (2.1) has been taken as the fitness function.

To inspect the performance of the metaheuristic techniques the standard test functions are used. A few of these with mathematical equations are shown in [84]. In this work, authors have selected five such standard test functions listed in Table 4.1 to assess the performance of the proposed algorithm of DG placement in terms of its quality and convergence.

A numeric value-based approach is used to inspect the comparative performance assessment of the proposed algorithm as compared with PSO and CRO techniques. In this way quality of the solution is measured by mean/average and Standard Deviation (SD) values. Table 4.2 sum up the convergence profile of the three optimization techniques (PSO-

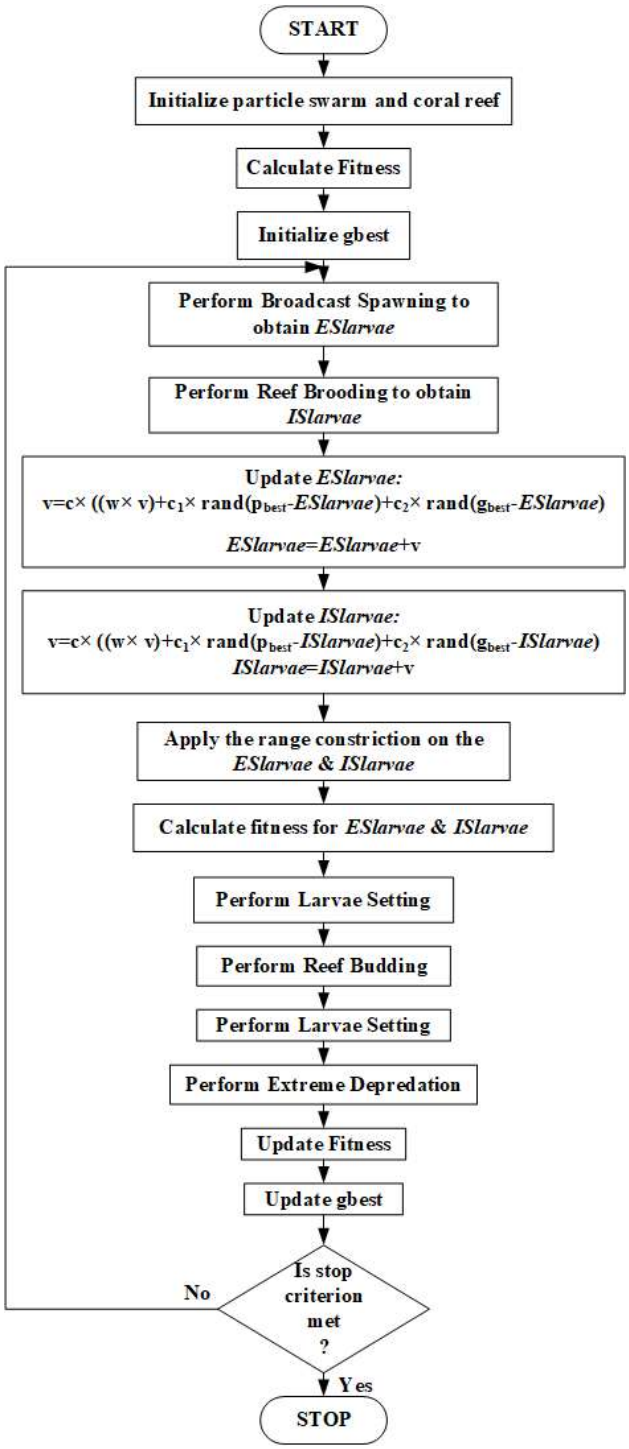


Fig. 4.8 Flowchart for optimal siting & sizing of DG using PSO-CRO

CRO, PSO, and CRO) for five test functions considered in this work. It is observed from Table 4.2 that the PSO-CRO approach is better compared to CRO and PSO irrespective of the test function considered due to the lower value of mean and SD values. To assess the search capability of PSO-CRO over PSO and CRO, simulations are carried out for dimension (D=5) and comparative convergence characteristics for PSO, CRO, and PSO-CRO algorithms for five test functions considered are shown in Fig. 4.9. It is observed from Fig. 4.9 that the PSO-CRO algorithm has better convergence characteristic over PSO and CRO.

Table 4.1 Representation of test functions

| Test function | Formulation | Characteristics | Range | $f_{min}$ |
|---|---|---|---|---|
| Sphere | $F_1$=$\sum_{i=1}^{D} x_i^2$ | US | [-100 100] | 0 |
| Rosenbrock | $F_2$=$\sum_{i=1}^{D-1} 100(x_{i+1}-x_i^2)^2$+$(1-x_i)^2$ | UN | [-30 30] | 0 |
| Rastrigin | $F_3$=10D+$\sum_{i=1}^{D} (x_i^2 - 10cos2\pi x(i))$ | MS | [-5.12 5.12] | 0 |
| Ackley | $F_4$=$-20\exp(-0.2\sqrt{\frac{1}{D}\sum_{i=1}^{D} x_i^2}) - \exp(\frac{1}{D}\sum_{i=1}^{D} cos2\pi x_i) + 20 + \exp 1$ | MN | [-32 32] | 0 |
| Griewank | $F_5 = \frac{1}{4000}\sum_{i=1}^{D} x_i^2 - \prod_{i=1}^{D} cos(\frac{x_i}{\sqrt{i}}) + 1$ | MN | [-600 600] | 0 |

## 4.4 Result and Discussion

### 4.4.1 33-Bus IEEE Network

The first test system is the 33-bus IEEE network on which the proposed approach and other optimization algorithms are tested for optimal siting and sizing of Type-1, Type-2 & Type-3 DG with one DG considered at a time. This system has a net real and reactive power demand of 3.72 MW and 2.3 MVAr, respectively. It has 33 buses and 32 branches. The details of the system are shown in Appendix A. On performing the load flow, the real and reactive power losses of the system were obtained as 210.9983 kW and 135.14 kVAr, respectively.

The optimal location of Type-1, Type-2 and Type-3 DG were obtained using the PSO-CRO algorithm minimizing the power loss. The maximum permissible DG size for

Table 4.2 Comparative performance assessment of PSO, CRO, and PSO-CRO algorithms on test functions

| Functions | Techniques | Best value | Worst value | Average | SD |
|---|---|---|---|---|---|
| $F_1$ | PSO-CRO | 0 | 5.74E-78 | **4.42E-24** | **3.12E-23** |
| | CRO | 2.26E-16 | 0.713385 | 1.43E-02 | 0.100882 |
| | PSO | 6.10E-19 | 0.000482 | 1.03E-05 | 6.82E-05 |
| $F_2$ | PSO-CRO | 9.15E-08 | 1.29E-07 | **1.54E-07** | **1.24E-07** |
| | CRO | 0.01066 | 3.991414 | 2.83E-01 | 0.940966 |
| | PSO | 3.73E-05 | 0.000935 | 2.28E-04 | 0.000129 |
| $F_3$ | PSO-CRO | 0 | 7.11E-15 | **7.58E-08** | **8.67E-09** |
| | CRO | 0.01818 | 8.9546 | 1.89043 | 1.585944 |
| | PSO | 1.63E-07 | 0.99498 | 2.22901 | 1.964816 |
| $F_4$ | PSO-CRO | 8.88E-16 | 7.99E-15 | **4.09E-15** | **1.79E-15** |
| | CRO | 5.12E-05 | 0.001508 | 5.39E-04 | 0.000336 |
| | PSO | 4.39E-05 | 0.000347 | 1.90E-04 | 9.78E-05 |
| $F_5$ | PSO-CRO | 0 | 8.88E-16 | **5.52E-15** | **1.42E-14** |
| | CRO | 5.73E-07 | 0.001274 | 0.000589 | 0.000328 |
| | PSO | 5.73E-07 | 0.000128 | 1.03E-05 | 9.60E-06 |

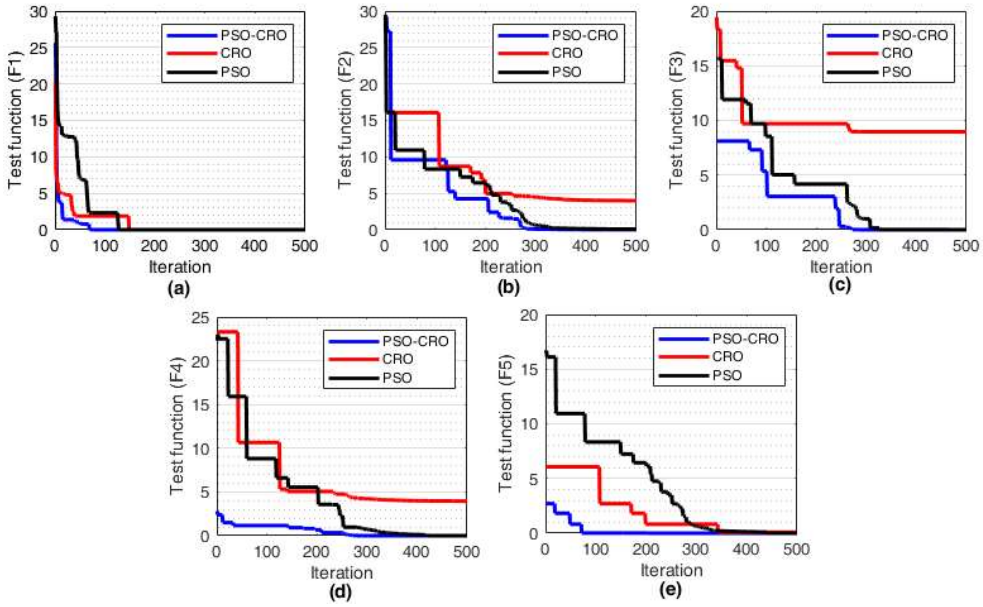


Fig. 4.9 Convergence characteristic comparison of PSO-CRO, CRO & PSO on a linear scale for dimension D=5 **(a)** Sphere, **(b)** Rosenbrock, **(c)** Rastrigin, **(d)** Ackley, **(e)** Griewank

Type-1, Type-2, and Type-3 DG were obtained as 3.931 MW, 2.435 MVAr, and 4.624 MVA, respectively satisfying DG constraints presented in Section 2.2.5 (Chapter-2) and Section 3.2 (Chapter-3). However, considering practical limitations maximum permissible size of Type-1, Type-2, and Type-3 DG were taken as 4 MW, 2.5 MVAr, and 4.5 MVA, respectively. Fig. 4.10 presents the size of Type-1, Type-2 & Type-3 DG for placement at each bus with minimum power loss. Figure 4.11 gives the system power loss corresponding to the optimal size of Type-1, Type-2 & Type-3 DG placement at each bus. It is observed from Fig. 4.10 and Fig. 4.11 that the placement of Type-1 DG of 2.5751 MW at bus-6, Type-2 DG of 1.2559 MVAr at bus-30 and Type-3 DG of 3.0985 MVA at bus-6 results in the power loss of 110.9856 kW, 150.8992 kW, and 67.0088 kW, respectively which corresponds to lowest power loss compared to DG placement at other buses. Therefore, bus-6, bus-30, and bus-6 were considered as optimal locations for DG placement with their size taken as 2.5940 MW, 1.2590 MVAr, and 3.0999 MVA, respectively. Though optimal DG sizes obtained by PSO-CRO algorithm are representing impractical values, these have been used in this work to compare the outcome of the proposed PSO-CRO algorithm with other algorithms of DG placement.

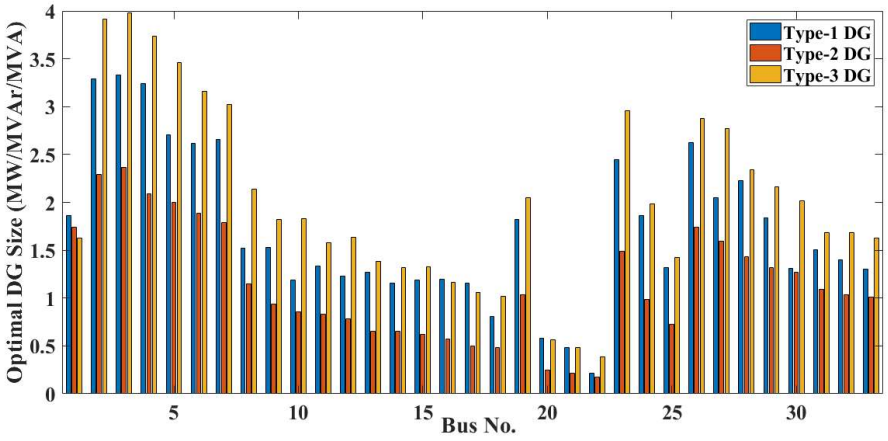


Fig. 4.10 Optimal size of DGs at each bus in 33-bus IEEE network using PSO-CRO

Table 4.3 presents the optimal location and size of Type-1, Type-2, and Type-3 DG obtained through 50 runs of PSO-CRO, PSO, CRO, GSA, PSO-GSA, PSO-GWO, CONOPT

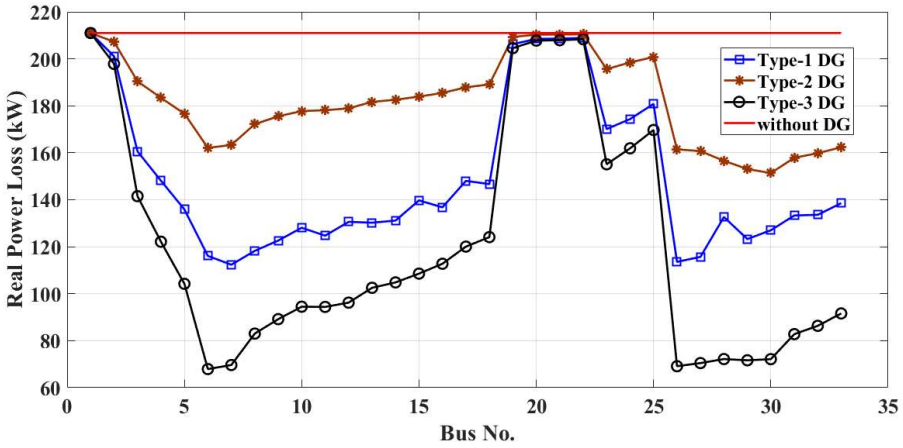


Fig. 4.11 System power loss for optimal DG size at each bus in 33-bus IEEE network using PSO-CRO

SOLVER of GAMS and few other approaches available in the literature. It is observed from Table 4.3 that the PSO-CRO approach gives better optimal solutions for placement of DG than PSO, CRO, GSA, PSO-GSA, PSO-GWO, CONOPT SOLVER and a few other existing approaches as power loss is minimum with DG placement by the proposed approach compared to other existing approaches.

Statistical analysis has been carried out to further validate the effectiveness of the proposed approach of DG placement. Figure 4.12, Fig. 4.13 & Fig. 4.14 depict the box plot for 50 runs of PSO, CRO, and proposed PSO-CRO algorithm for placement of Type-1, Type-2 & Type-3 DG, respectively. It is observed from Fig. 4.12, Fig. 4.13, and Fig. 4.14 that DG size obtained by the proposed PSO-CRO approach have much smaller variations from its mean value over 50 runs considered compared to PSO and CRO algorithms.

Table 4.4 shows the first quartile (i.e. Q1), second quartile/median (i.e. Q2), and third quartile (i.e. Q3) values with respect to PSO, CRO, and PSO-CRO algorithm for Type-1, Type-2 & Type-3 DG. It is observed from Table 4.4 that the median ($Q_2$) value is most close to $Q_1$ and $Q_3$ values if Type-1, Type-2, and Type-3 DG placement are considered using the proposed PSO-CRO algorithm.

Table 4.3 Performance analysis of optimal DG integration in 33-bus IEEE network

| Method | Type-1 DG | | | Type-2 DG | | | Type-3 DG | | |
|---|---|---|---|---|---|---|---|---|---|
| | Bus No. | DG Size (MW) | Power loss (kW) | Bus No. | DG Size (MVAr) | Power loss (kW) | Bus No. | DG Size (MVA) | Power loss (kW) |
| Proposed (PSO-CRO) | 6 | 2.5751 | **110.9856** | 30 | 1.2559 | **150.8992** | 6 | 3.0985 | **67.0088** |
| PSO | 6 | 2.5338 | 111.0738 | 30 | 1.2483 | 151.3820 | 6 | 3.0650 | 67.8965 |
| CRO | 6 | 2.5950 | 111.0302 | 30 | 1.2625 | 151.3794 | 6 | 3.1404 | 67.8894 |
| GSA | 6 | 2.2564 | 111.1422 | 30 | 2.3334 | 151.3788 | 6 | 2.9252 | 67.8831 |
| PSO-GSA | 6 | 2.5902 | 111.0299 | 30 | 1.2579 | 151.3787 | 6 | 3.1061 | 67.8738 |
| PSO-GWO | 6 | 2.5973 | 111.0306 | 30 | 1.2614 | 151.3791 | 6 | 3.1082 | 67.8739 |
| CONOPT SOLVER [106] | 6 | 2.5655 | 111.0000 | 30 | 1.2578 | 150.9980 | 6 | 3.0785 | 67.8000 |
| HGWO [107] | 6 | 2.5900 | 111.0180 | 30 | 1.2580 | 151.3600 | 6 | 3.1600 | 67.8550 |
| Hybrid [108] | 6 | 2.4900 | 111.1700 | 30 | 1.2300 | 151.4100 | 6 | 3.0280 | 67.9370 |
| MINLP [107] | 6 | 2.5900 | 111.0180 | - | - | - | 6 | 3.1050 | 67.8550 |
| EA OPF [109] | 6 | 2.5900 | 111.0200 | - | - | - | 6 | 3.1190 | 67.8600 |
| EA [109] | 6 | 2.5300 | 111.0700 | - | - | - | 6 | 3.1190 | 67.8700 |
| IA [106] | 6 | 2.6000 | 111.1000 | - | - | - | 6 | 3.1070 | 67.9000 |
| Exhaustive OPF [109] | 6 | 2.5900 | 111.0200 | - | - | - | - | - | - |

'-' represents the types of DGs are not considered in the corresponding reference

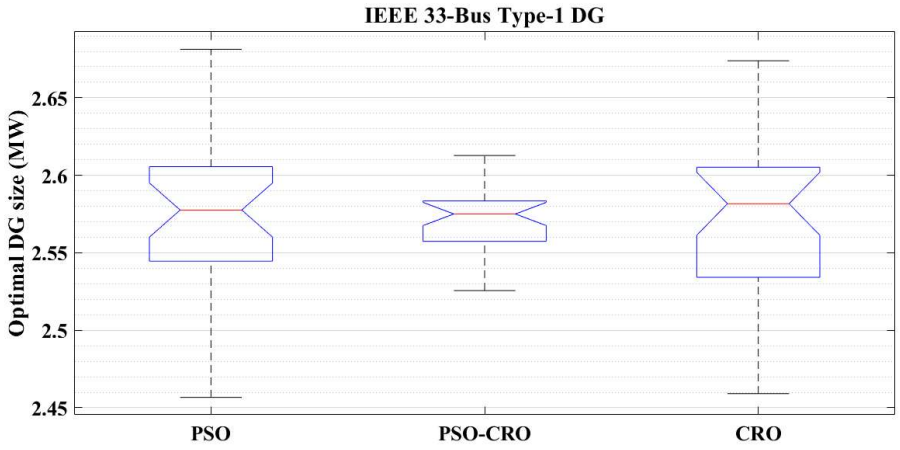


Fig. 4.12 Box plot for Type-1 DG

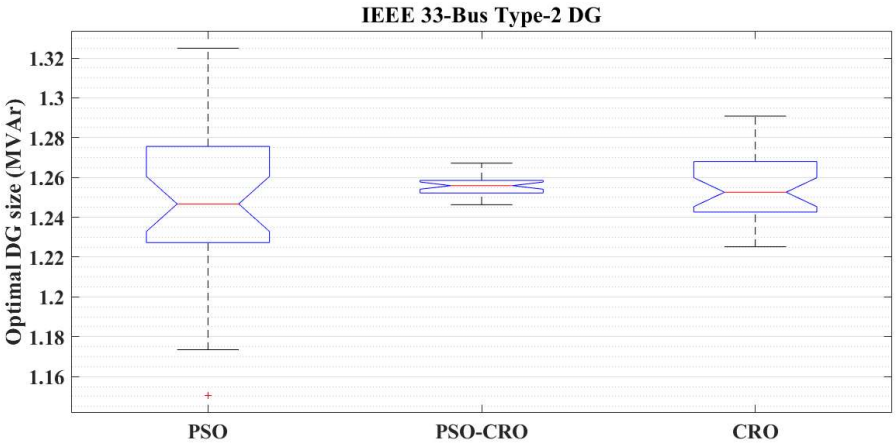


Fig. 4.13 Box plot for Type-2 DG

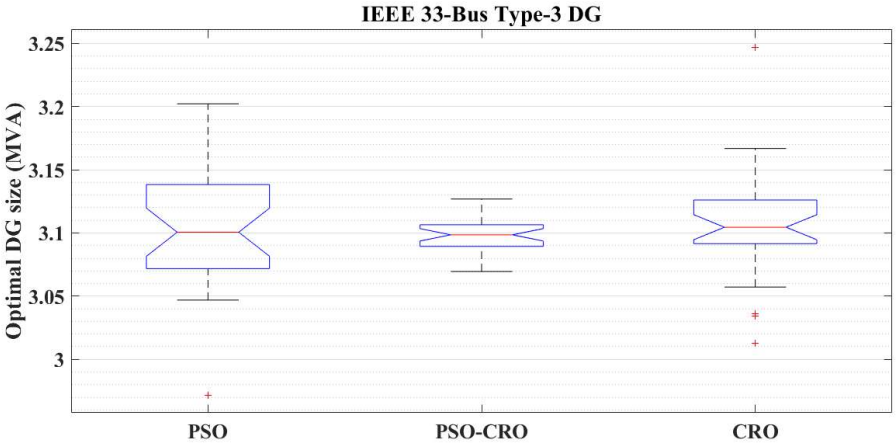


Fig. 4.14 Box plot for Type-3 DG

Table 4.4 First quartile (i.e. Q1), second quartile/median (i.e. Q2), and third quartile (i.e. Q3) values for 33-bus RDS.

| DG Type | 33-bus IEEE network | | | | | | | | |
|---|---|---|---|---|---|---|---|---|---|
| | PSO | | | CRO | | | PSO-CRO | | |
| | Q3 | Q2 | Q1 | Q3 | Q2 | Q1 | Q3 | Q2 | Q1 |
| **Type-1** | 2.6056 | 2.5776 | 2.5446 | 2.6052 | 2.5816 | 2.5342 | 2.5835 | **2.5751** | 2.5574 |
| **Type-2** | 1.2756 | 1.2467 | 1.2273 | 1.2675 | 1.2526 | 1.2426 | 1.2585 | **1.2559** | 1.2522 |
| **Type-3** | 3.0718 | 3.1006 | 3.1383 | 3.1261 | 3.1046 | 3.0915 | 3.1065 | **3.0985** | 3.0894 |

The voltage profile for placement of Type-1, Type-2, and Type-3 DG by the proposed approach as well as the voltage profile for without DG case has been shown in Fig. 4.15. It is observed from Fig. 4.15 that though the placement of all three types of DG improves the voltage profile of the system, Type-3 DG is most effective in voltage profile improvement compared to the other two types of DG considered in this work. This may be due to real as well as reactive power injection by Type-3 DG as the distribution network needs reactive as well real power compensation to improve its voltage profile due to its high R/X ratio.

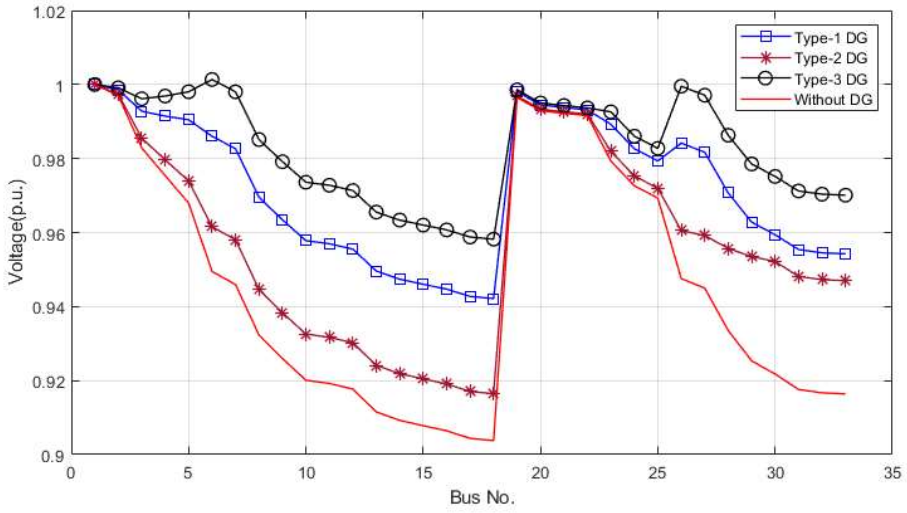


Fig. 4.15 Voltage profile of 33-bus RDS with and without DGs using PSO-CRO

The average computational time for 50 runs of different algorithms is shown in Table 4.5. It is observed from Table 4.5 that the proposed PSO-CRO optimization approach results in the least computational time over some other existing metaheuristic optimization approaches under optimal integration of all the three types of DGs considered in this work.

Table 4.5 Average computational time for 33-bus IEEE network.

| 33-bus IEEE network | | | |
|---|---|---|---|
| **Optimization technique** | **Computational time (Sec.)** | | |
| | **Type-1 DG placement** | **Type-2 DG placement** | **Type-3 DG placement** |
| PSO | 5.8151 | 5.1301 | 5.1446 |
| CRO | 9.4136 | 9.2273 | 9.3019 |
| GSA | 13.1209 | 13.4714 | 13.5001 |
| PSO-GSA | 12.4822 | 12.8619 | 13.0482 |
| PSO-GWO | 5.1706 | 5.2592 | 5.1528 |
| **PSO-CRO** | **1.8402** | **1.8991** | **1.8896** |

### 4.4.2 69-Bus IEEE Network

The second test bed is 69-bus IEEE network on which the proposed approach and other optimization algorithms are tested for optimal siting and sizing of Type-1, Type-2 & Type-3 DG with one DG considered at a time. This system has a net real and reactive power demand of 3.80 MW and 2.69 MVAr, respectively. The details of the system are shown in Appendix B. Power flow study shows that the real and reactive powers of the system are obtained as 225.002 kW and 102.525 kVAr, respectively.

The optimal location of Type-1, Type-2, and Type-3 DG were obtained using the PSO-CRO algorithm minimizing the power loss. The maximum permissible DG size for Type-1, Type-2, and Type-3 DG were obtained as 4.025 MW, 2.793 MVAr, and 4.899 MVA respectively satisfying DG constraints presented in Section 2.2.5 (Chapter-2) and Section 3.2 (Chapter-3). However, considering practical limitations maximum permissible size of Type-1, Type-2, and Type-3 DG were taken as 4 MW, 3 MVAr, and 5 MVA, respectively. Fig. 4.16 presents the size of Type-1, Type-2 & Type-3 DG for placement at each bus with minimum power loss. Figure 4.17 gives the system power loss corresponding to the optimal size of Type-1, Type-2 & Type-3 DG placement at each bus. It is observed from Fig. 4.16 and Fig. 4.17 that placement of Type-1 DG of 1.8666 MW at bus-61, Type-2 DG of 1.3285 MVAr at bus-61 and Type-3 DG of 2.2396 MVA at bus-61 results in the power loss of 83.0014 kW, 151.9934 kW and 24.0011 kW, respectively which corresponds to lowest power loss compared to DG placement at other buses. Therefore, bus-61 was considered as the optimal location for placement of all three types of DGs considered in this work with their size taken as 1.8666 MW, 1.3285 MVAr, and 2.2396 MVA for

Type-1, Type-2, and Type-3 DG, respectively. Though optimal DG sizes obtained by the PSO-CRO algorithm are representing impractical values, these have been used in this work to compare the outcome of proposed the PSO-CRO algorithm with other algorithms of DG placement.

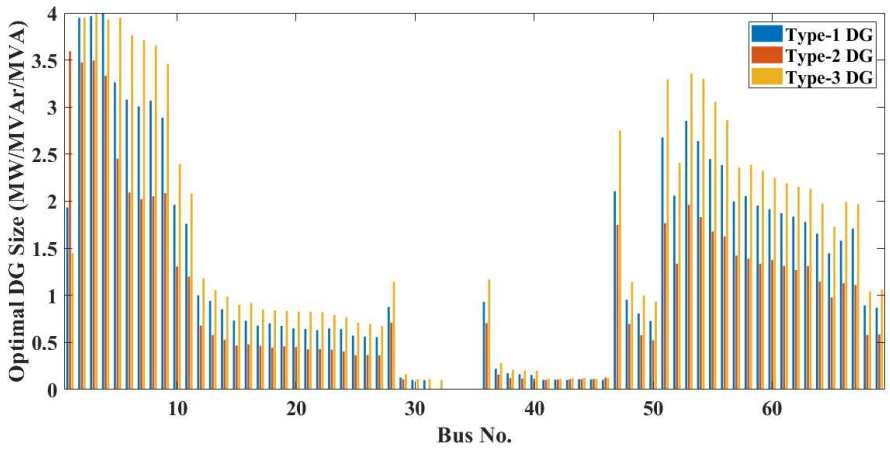


Fig. 4.16 Optimal size of DGs at each bus in 69-bus IEEE network using PSO-CRO

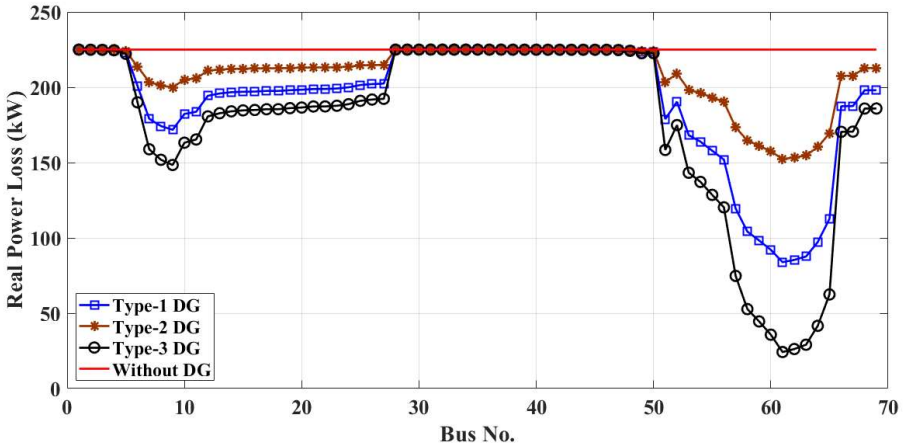


Fig. 4.17 System power loss for optimal DG size at each bus in 69-bus IEEE network using PSO-CRO

Table 4.6 presents the optimal location and size of Type-1, Type-2, and Type-3 DG obtained through 50 runs of PSO-CRO, PSO, CRO, GSA, PSO-GSA, PSO-GWO, CONOPT SOLVER of GAMS and few other approaches available in the literature. It is observed

Table 4.6 Performance analysis of optimal DG integration in 69-bus IEEE network

| Method | Type-1 DG | | | Type-2 DG | | | Type-3 DG | | |
|---|---|---|---|---|---|---|---|---|---|
| | DG Size (MW) | Power loss (kW) | Bus No. | DG Size (MVAr) | Power loss (kW) | Bus No. | DG Size (MVA) | Power loss (kW) | Power loss (kW) |
| Proposed (PSO-CRO) | 61 | 1.8666 | **83.0014** | 61 | 1.3285 | **151.9934** | 61 | 2.2396 | **24.0011** |
| PSO | 61 | 2.0264 | 84.0400 | 61 | 1.3965 | 152.5922 | 61 | 2.2392 | 24.1675 |
| CRO | 61 | 1.9627 | 84.2092 | 61 | 1.3625 | 152.4525 | 61 | 2.2400 | 24.1676 |
| GSA | 61 | 3.0758 | 84.3900 | 61 | 1.6827 | 152.4034 | 61 | 2.5448 | 24.1720 |
| PSO-GSA | 61 | 1.8685 | 83.9013 | 61 | 1.3272 | 152.4033 | 61 | 2.2386 | 24.1675 |
| PSO-GWO | 61 | 1.8572 | 83.9058 | 61 | 1.3282 | 152.4214 | 61 | 2.2405 | 24.1676 |
| CONOPT SOLVER [106] | 61 | 1.8877 | 83.1500 | 62 | 1.3080 | 152.6790 | 61 | 2.2626 | 23.1200 |
| CPLS [106] | 61 | 1.8500 | 83.1500 | - | - | - | 61 | 2.2000 | 27.9100 |
| HGWO [107] | 61 | 1.8720 | 83.2220 | 61 | 1.3300 | 152.0410 | 61 | 2.2460 | 23.1600 |
| Hybrid [108] | 61 | 1.1810 | 83.3720 | 61 | 1.2900 | 152.1020 | 61 | 2.2000 | 23.9200 |
| MINLP [107] | 61 | 1.8700 | 83.2220 | - | - | - | 61 | 2.2440 | 23.1600 |
| EA OPF [109] | 61 | 1.8700 | 83.2300 | - | - | - | 61 | 2.2290 | 23.1700 |
| EA [109] | 61 | 1.8780 | 83.2300 | - | - | - | 61 | 2.2900 | 23.2600 |
| Exhaustive OPF [109] | 61 | 1.8700 | 83.2300 | - | - | - | - | - | - |

'-' represents the types of DGs are not considered in the corresponding reference

from Table 4.6 that the PSO-CRO approach gives better optimal solutions for placement of DG than PSO, CRO, GSA, PSO-GSA, PSO-GWO, CONOPT SOLVER, and a few other existing approaches as power loss is minimum with DG placement by proposed approach compared to other existing approaches.

Statistical analysis has been carried out to further validate the effectiveness of the proposed approach of DG placement. Fig. 4.18, Fig. 4.19 & Fig. 4.20 depict the box plot for 50 runs of PSO, CRO, and proposed PSO-CRO algorithm for placement of Type-1, Type-2 & Type-3 DG, respectively. It is observed from Fig. 4.18, Fig. 4.19 & Fig. 4.20 that DG sizes obtained by the proposed PSO-CRO approach have much smaller variations from its mean values over 50 runs considered compared to PSO and CRO algorithms.

Table 4.7 shows the first quartile (i.e. Q1), second quartile/median (i.e. Q2), and third quartile (i.e. Q3) values with respect to PSO, CRO, and PSO-CRO algorithm for Type-1, Type-2 & Type-3 DG. It is observed from Table 4.7 that the median ($Q_2$) value is most close to $Q_1$ and $Q_3$ values if Type-1, Type-2, and Type-3 DG placement are considered using the proposed PSO-CRO algorithm.

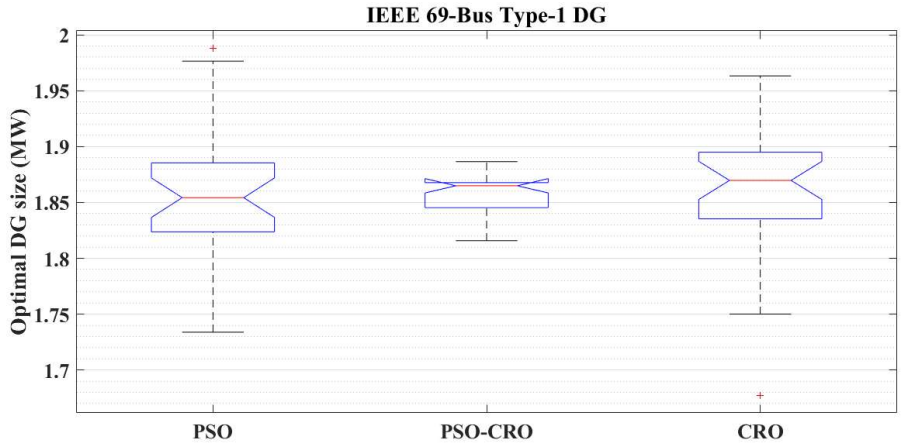


Fig. 4.18 Box plot for Type-1 DG

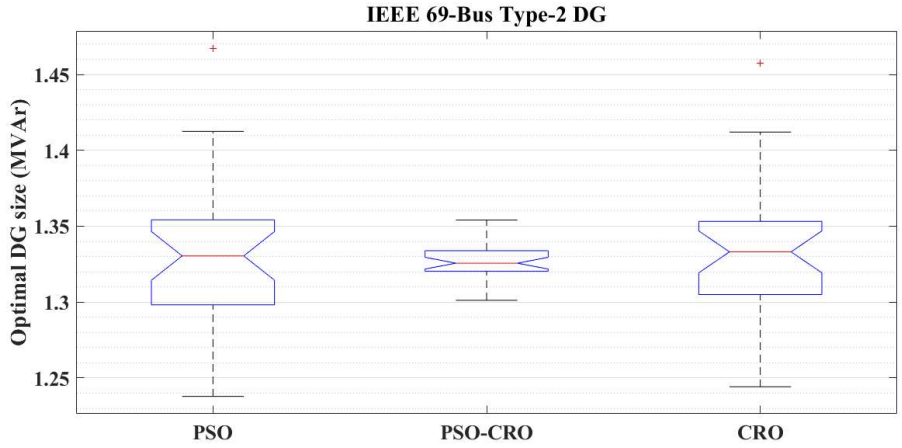


Fig. 4.19 Box plot for Type-2 DG

The voltage profile for placement of Type-1, Type-2, and Type-3 DGs by the proposed approach as well as voltage profile without DG case has been shown in Fig. 4.21. It is observed from Fig. 4.21 that though the placement of all three types of DG improves the voltage profile of the system, Type-3 DG is most effective in voltage profile improvement compared to the other two types of DG considered in this work. This may be due to real as well as reactive power injection by Type-3 DG as the distribution network needs reactive as well real power compensation to improve its voltage profile due to its high R/X ratio.

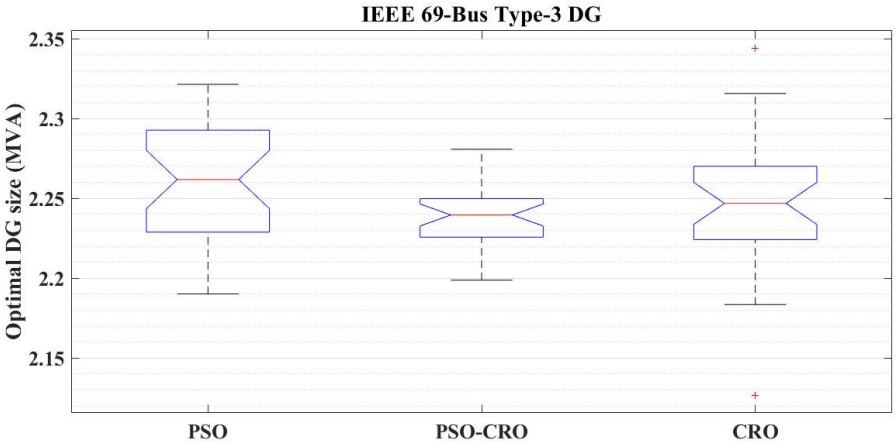


Fig. 4.20 Box plot for Type-3 DG

Table 4.7 First quartile (i.e. Q1), second quartile/median (i.e. Q2), and third quartile (i.e. Q3) values for 69-bus RDS

| DG Type | 69-Bus RDS | | | | | | | | |
|---|---|---|---|---|---|---|---|---|---|
| | PSO | | | CRO | | | PSO-CRO | | |
| | Q3 | Q2 | Q1 | Q3 | Q2 | Q1 | Q3 | Q2 | Q1 |
| **Type-1** | 1.8854 | 1.8542 | 1.8237 | 1.8949 | 1.8697 | 1.8353 | 1.8677 | **1.8666** | 1.8453 |
| **Type-2** | 1.3542 | 1.3304 | 1.2982 | 1.3532 | 1.3331 | 1.3048 | 1.3339 | **1.3285** | 1.3204 |
| **Type-3** | 2.2927 | 2.2618 | 2.2289 | 2.2701 | 2.2469 | 2.2242 | 2.2498 | **2.2396** | 2.2257 |

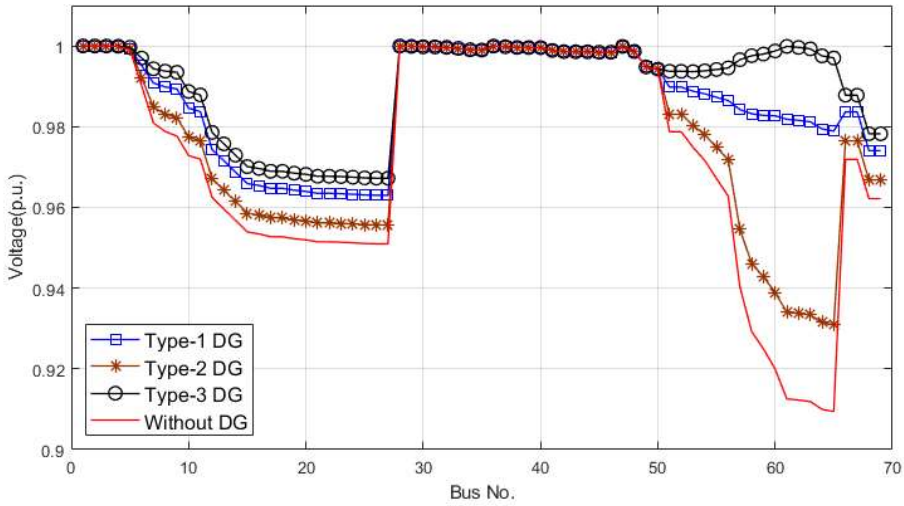


Fig. 4.21 Voltage profile of 69-bus RDS with and without DGs using PSO-CRO

The average computational time for 50 runs of different algorithms is shown in Table 4.8. It is observed from Table 4.8 that the proposed PSO-CRO optimization approach results in minimum computational time compared to some other existing metaheuristic optimization approaches under the placement of all the three types of DGs considered in the work.

Table 4.8 Average computational time for 69-bus IEEE network.

| **69-bus IEEE network** | | | |
|---|---|---|---|
| **Optimization technique** | **Computational time (Sec.)** | | |
| | **Type-1 DG placement** | **Type-2 DG placement** | **Type-3 DG placement** |
| PSO | 33.9360 | 33.9799 | 35.0513 |
| CRO | 62.8101 | 62.9990 | 62.9647 |
| GSA | 43.1392 | 43.1562 | 45.0636 |
| PSO-GSA | 42.4069 | 42.0382 | 42.1048 |
| PSO-GWO | 33.7171 | 35.4585 | 34.3210 |
| **PSO-CRO** | **8.1376** | **8.2098** | **8.2408** |

### 4.4.3 118-Bus Radial Distribution System

The third test bed is 118-bus IEEE network on which the proposed approach and other optimization algorithms are tested for optimal siting and sizing of Type-1, Type-2 & Type-3 DG with one DG considered at a time. This system has a net real and reactive power demand 22.709 MW and 17.041 MVAr, respectively. The details of the system are given in Appendix C. On performing the load flow, the real and reactive power losses of the system were obtained as 1298.0916 kW and 978.736 kVAr, respectively.

The optimal location of Type-1, Type-2, and Type-3 DG were obtained using the PSO-CRO algorithm minimizing the power loss. The maximum permissible DG sizes for Type-1, Type-2, and Type-3 DG were obtained as 24.007 MW, 18.019 MVAr, and 30.017 MVA, respectively satisfying DG constraints presented in Section 2.2.5 (Chapter-2) and Section 3.2 (Chapter-3). However, considering practical limitations maximum permissible size of Type-1, Type-2, and Type-3 DG were taken as 4 MW, 4 MVAr, and 5 MVA, respectively. Fig. 4.22 presents the size of Type-1, Type-2 & Type-3 DG for placement at each bus with minimum power loss. Fig. 4.23 gives the system power loss corresponding

to the optimal size of Type-1, Type-2 & Type-3 DG placement at each bus. It is observed from Fig. 4.22 and Fig. 4.23 that placement of Type-1 DG of 3.0073 MW at bus-71, Type-2 DG of 2.3000 MVAr at bus-110, and Type-3 DG of 3.4861 MVA at bus-71 results in power loss of 824.8902 kW, 916.9917 kW, and 746.9887 kW, respectively which corresponds to lowest power loss compared to DG placement at other buses. Therefore, bus-71, bus-110, and bus-71 were considered as optimal locations for DG placement with their size taken as 3.0073 MW, 2.3000 MVAr, and 3.4861 MVA, respectively. Though optimal DGs size obtained by the PSO-CRO algorithm are representing impractical values, these have been used in this work to compare the outcome of the proposed PSO-CRO algorithm with other algorithms of DG placement.

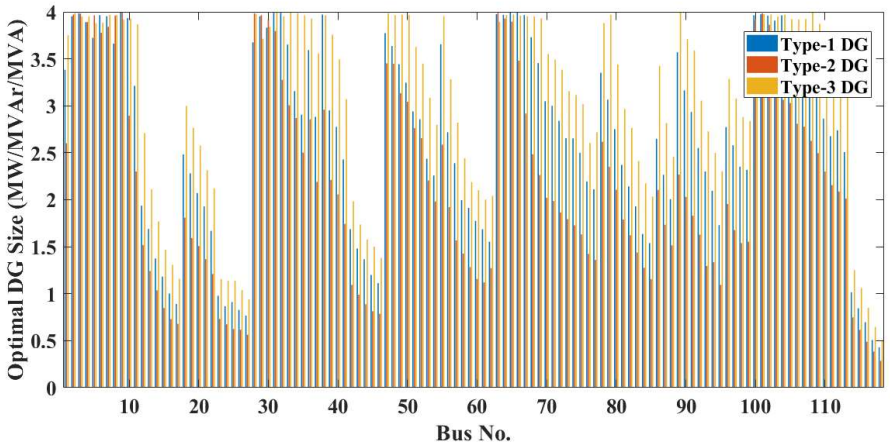


Fig. 4.22 Optimal size of DGs at each bus in 118-bus IEEE network using PSO-CRO

Table 4.9 presents the optimal location and size of Type-1, Type-2, and Type-3 DG obtained through 50 runs of PSO-CRO, PSO, CRO, GSA, PSO-GSA, PSO-GWO, CONOPT SOLVER of GAMS and few other approaches available in the literature. It is observed from Table 4.9 that the PSO-CRO approach gives better optimal solutions for placement of DG than PSO, CRO, GSA, PSO-GSA, PSO-GWO, CONOPT SOLVER, and a few other existing approaches as power loss is minimum with DG placement by proposed approach compared to other existing approaches.

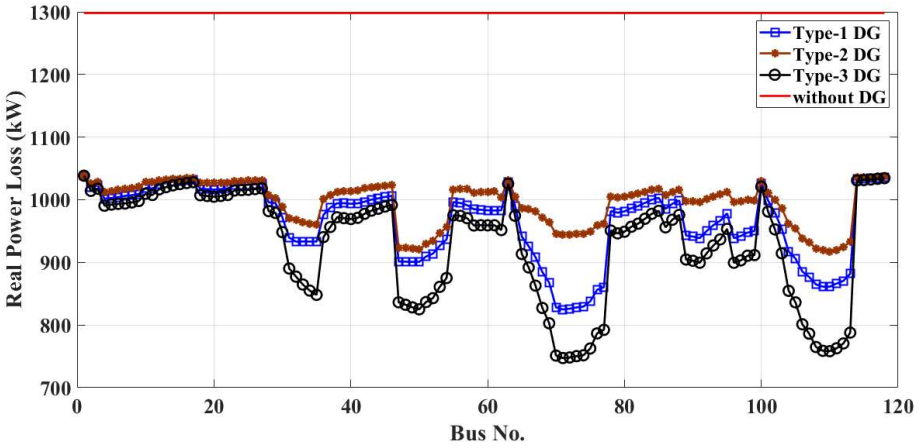


Fig. 4.23 System power loss for optimal DG size at each bus in 118-bus IEEE network using PSO-CRO

Statistical analysis has been carried out to further validate the effectiveness of the proposed approach of DG placement. Fig. 4.24, Fig. 4.25, & Fig. 4.26 depict the box plot for 50 runs of PSO, CRO, and proposed PSO-CRO algorithm for placement of Type-1, Type-2 & Type-3 DG, respectively. It is observed from Fig. 4.24, Fig. 4.25, & Fig. 4.26 that DG size obtained by the proposed PSO-CRO approach has much smaller variations from its mean value over 50 runs considered compared to PSO and CRO algorithms.

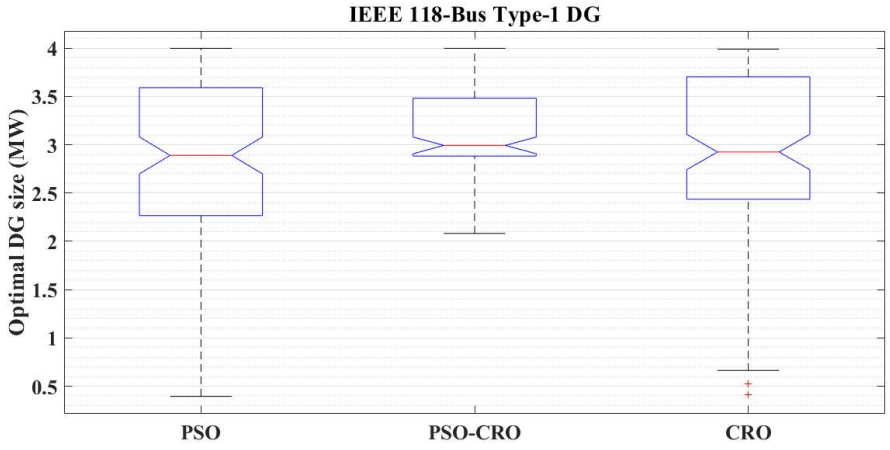


Fig. 4.24 Box plot for Type-1 DG

Table 4.9 Performance analysis of optimal DG integration in 118-bus IEEE network

| Method | Type-1 DG | | | Type-2 DG | | | Type-3 DG | | |
|---|---|---|---|---|---|---|---|---|---|
| | DG Size (MW) | Power loss (kW) | Bus No. | DG Size (MVAr) | Power loss (kW) | Bus No. | DG Size (MVA) | Power loss (kW) | Power loss (kW) |
| Proposed (PSO-CRO) | 71 | 3.0073 | **824.8902** | 110 | 2.3000 | **916.9917** | 71 | 3.4861 | **746.9887** |
| PSO | 71 | 2.9200 | 825.0315 | 110 | 2.4902 | 917.0693 | 71 | 3.5568 | 747.2363 |
| CRO | 71 | 2.9839 | 825.1003 | 110 | 2.5629 | 918.1537 | 71 | 3.8937 | 747.5961 |
| GSA | 71 | 3.9014 | 825.0089 | 110 | 3.5435 | 917.0991 | 71 | 2.9635 | 747.2769 |
| PSO-GSA | 71 | 2.8497 | 825.0101 | 110 | 2.5366 | 917.1537 | 71 | 3.8766 | 747.2283 |
| PSO-GWO | 71 | 2.9987 | 825.1100 | 110 | 2.4344 | 917.0897 | 71 | 3.9846 | 747.2296 |
| CONOPT SOLVER [106] | 79 | 3.0212 | 885.1465 | 114 | 2.7392 | 934.4086 | 68 | 4.3033 | 747.0005 |
| HSA-PABC [39] | 70 | 3.0500 | 1021.0900 | - | - | - | - | - | - |
| SOS [39] | 70 | 3.0482 | 1021.0890 | - | - | - | - | - | - |
| WOA [39] | 113 | 2.7040 | 1092.4600 | - | - | - | - | - | - |
| PIPSO-SQP [39] | 72 | 2.9785 | 1016.8000 | - | - | - | - | - | - |

'-' represents the types of DGs are not considered in the corresponding reference

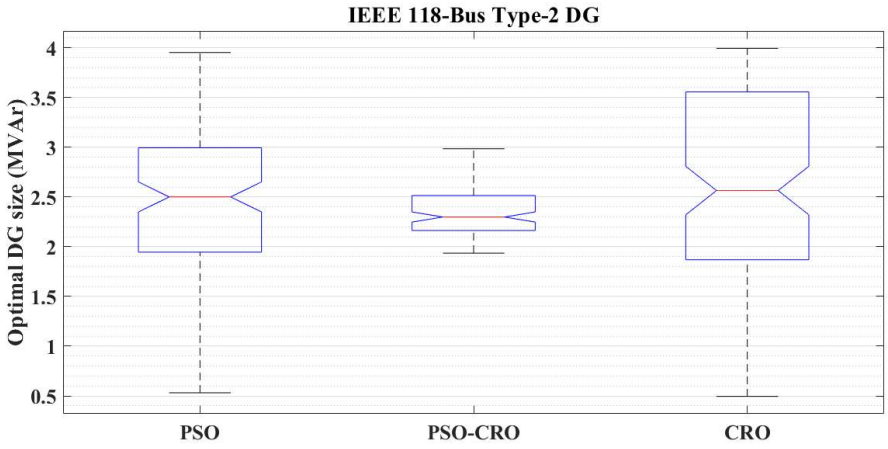


Fig. 4.25 Box plot for Type-2 DG

Table 4.10 shows the first quartile (i.e. Q1), second quartile/median (i.e. Q2), and third quartile (i.e. Q3) values with respect to PSO, CRO, and PSO-CRO algorithm for Type-1, Type-2  Type-3 DG. It is observed from Table 4.10 that the median ($Q_2$) value is most close to $Q_1$ and $Q_3$ values if Type-1, Type-2, and Type-3 DG placement are considered using the proposed PSO-CRO algorithm.

The voltage profile for placement of Type-1, Type-2, and Type-3 DGs by the proposed approach as well as the voltage profile without DG case has been shown in Fig. 4.27. It is

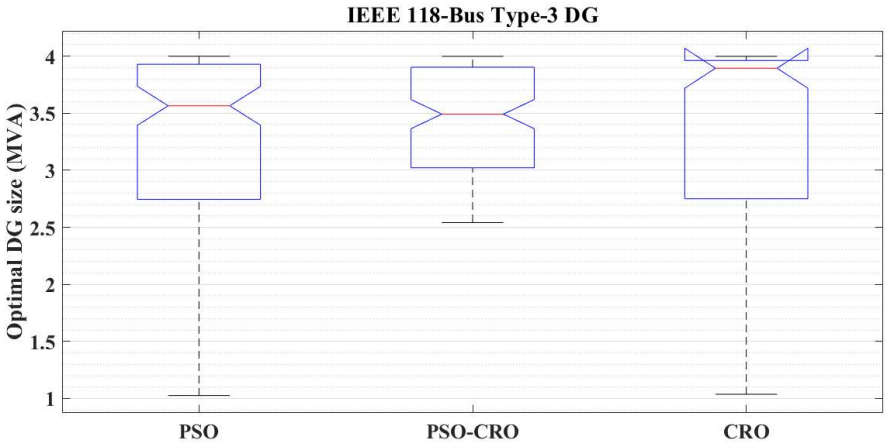


Fig. 4.26 Box plot for Type-3 DG

Table 4.10 First quartile (i.e. Q1), second quartile/median (i.e. Q2), and third quartile (i.e. Q3) values for 118-bus RDS

| DG Type | 118-Bus RDS | | | | | | | | |
|---|---|---|---|---|---|---|---|---|---|
| | PSO | | | CRO | | | PSO-CRO | | |
| | Q3 | Q2 | Q1 | Q3 | Q2 | Q1 | Q3 | Q2 | Q1 |
| **Type-1** | 3.5920 | 2.9200 | 2.2678 | 3.7048 | 2.9839 | 2.4362 | 3.4823 | **3.0073** | 2.8838 |
| **Type-2** | 2.9939 | 2.4902 | 1.9452 | 3.5568 | 2.5629 | 1.8681 | 2.5150 | **2.3000** | 2.1628 |
| **Type-3** | 3.9285 | 3.5568 | 2.7451 | 3.9615 | 3.8937 | 2.7494 | 3.9026 | **3.4861** | 3.0212 |

observed from Fig. 4.27 that though the placement of all three types of DG improves the voltage profile of the system, Type-3 DG is most effective in voltage profile improvement compared to the other two types of DG considered in this work. This may be due to real as well as reactive power injection by Type-3 DG as the distribution network needs reactive as well real power compensation to improve its voltage profile due to its high R/X ratio.

The average computational time for 50 runs of different algorithms is shown in Table 4.11. It is observed from Table 4.11 that the proposed PSO-CRO optimization approach results in the least computational time over some other existing metaheuristic optimization approach under optimal integration of all the three types of DGs considered in this work.

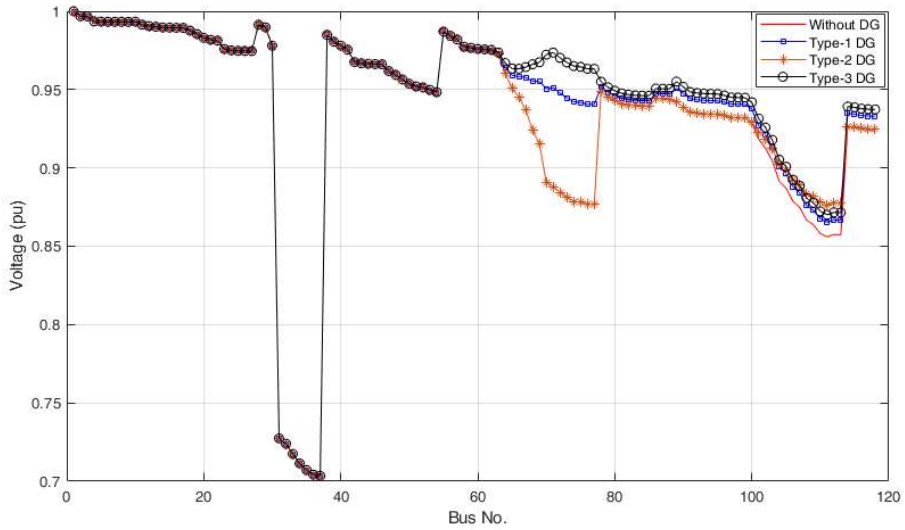


Fig. 4.27 Voltage profile of 118-bus RDS with and without DGs using PSO-CRO

Table 4.11 Average computational time for 118-bus IEEE network.

| **118-bus IEEE network** | | | |
|---|---|---|---|
| **Optimization technique** | **Computational time (Sec.)** | | |
| | **Type-1 DG placement** | **Type-2 DG placement** | **Type-3 DG placement** |
| PSO | 185.3673 | 185.8833 | 185.9187 |
| CRO | 376.9396 | 376.8467 | 376.7964 |
| GSA | 368.6843 | 368.8502 | 370.5487 |
| PSO-GSA | 203.6566 | 203.8932 | 205.5787 |
| PSO-GWO | 248.3372 | 245.7584 | 396.2382 |
| **PSO-CRO** | **153.5437** | **153.2579** | **153.3583** |

## 4.5 Summary

The novel approach based on the hybridization of PSO and CRO algorithms was proposed in this chapter for the optimal placement of distributed generators in distribution networks. The placement of Type-1, Type-2, and Type-3 DGs were considered with their optimal location and size obtained by the hybrid PSO-CRO algorithm. The idea behind this hybridization was to combine the high exploration capability of PSO and the excellent exploitation proficiency of CRO. The effectiveness of the proposed approach on DG placement was tested on three systems. Case studies performed on three test systems resulted in the lowest power loss with the proposed approach of DG placement compared

to a few other existing approaches. The DG size obtained by the proposed approach was close to its mean value for 50 runs of the algorithm. The proposed approach was shown to be computationally efficient, too, as the computation time involved in running the proposed algorithm of DG placement was much less compared to a few other existing approaches. The proposed approach of DG placement resulted in a significant enhancement in the voltage profile of the network. Type-3 was found to be most effective in voltage profile improvement compared to DGs of the other two types for three test systems considered in this work.

**********